Field Theoretic Study of Bilayer Membrane Fusion III: Membranes with Leaves of Different Composition

J. Y. Lee and M. Schick
Department of Physics, University of Washington, Seattle, Washington

ABSTRACT We extend previous work on homogeneous bilayers to calculate the barriers to fusion of planar bilayers that contain two different amphiphiles, a lamellar former and a hexagonal former, with different compositions of the two in each leaf. Self-consistent field theory is employed, and both standard and alternative pathways are explored. We first calculate these barriers as the amount of hexagonal former is increased equally in both leaves to levels appropriate to the plasma membrane of human red blood cells. We follow these barriers as the composition of hexagonal formers is then increased in the *cis* layer and decreased in the *trans* layer, again to an extent comparable to the biological system. We find that, while the fusion pathway exhibits two barriers in both the standard and alternative pathways, in both cases the magnitudes of these barriers are comparable to one another, and small, on the order of 13 k_BT. As a consequence, one expects that once the bilayers are brought sufficiently close to one another to initiate the process, fusion should occur rapidly.

INTRODUCTION

Despite the importance of membrane fusion to biological processes such as endocytosis, intracell trafficking, and viral infection, and despite the increased attention devoted to it, the process is still not well understood. In particular, it is unclear what the sequence of events along the path to fusion is, which of those events presents the greatest barrier to fusion, and what the magnitude of that barrier is.

The initial stages of the sequence are relatively clear (1,2). The membranes to be fused must be brought sufficiently close to one another, within a few nanometers. To do so, water must be removed, which takes energy. Presumably, this is provided by fusion proteins in biological systems, but can, in laboratory samples in which such proteins are absent, be provided simply by ordinary depletion forces (3). As a result of the decrease of water, the free energy per unit area of the system increases; in other words, the system is now under tension. The free energy can be reduced if the system sheds area. Fusion, which accomplishes this, is one possible response of the system to that tension. The next stage in the process is that, locally, some lipid tails in the membrane leaves which are closest to one another, i.e., the *cis* leaves, flip over and embed themselves in the hydrophobic environment of the *cis* leaf of the other bilayer, thereby forming a ''stalk'' (4), as depicted in Fig. 1 *a*. This process is consistent with experimental evidence ((1) and references therein), and has been seen directly in simulations of coarse-grained, microscopic, models of membranes (5–9).

The next stage is unclear, and several possibilities have been proposed. The original suggestion (4) was that the stalk expands radially from an axis perpendicular to the bilayers, as in Fig. 1 *b*. The *cis* layers retract, leaving a hemifusion diaphragm, which consists only of the leaves of the two membranes that were initially furthest from one another, the *trans* leaves. Note that membrane area has been reduced as the hemifusion diaphragm now consists only of two, *trans*, leaves in place of the original four, two *cis* and two *trans*. The appearance of a hole in this hemifusion diaphragm completes the formation of the fusion pore, Fig. 1 *c*. On the basis of phenomenological modeling similar to that employed earlier (4), a second scenario was suggested: that the pore forms without significant radial expansion of the stalk (10,11). A third possibility was revealed by simulations of coarse-grained, microscopic models (5,6,12). In this, which we denote the first stalk-hole mechanism, the stalk does not expand radially, but elongates asymmetrically. Its presence makes more favorable the formation nearby of a hole in either bilayer by reducing the line tension of the hole (13). The stalk then surrounds the hole, which also produces a hemifusion diaphragm, as in the standard stalk mechanism, but one consisting of a *cis* and *trans* layer of one of the original bilayers. The appearance of a second hole, this in the hemifusion diaphragm, then completes the fusion pore. A hemifusion diaphragm is also consistent with experimental evidence ((14) and references therein). In a variant of this mechanism, denoted the second stalk-hole mechanism, the second hole appears before the first is surrounded. The mobile stalk then surrounds them both forming the fusion pore. After formation of the fusion pore, the pore expands to further eliminate area and thus reduce the system's free energy. Simulations of coarse-grained, microscopic, models have observed the original mechanism (8,9,12), and also the stalk-hole mechanism (5–9,12). If the path to fusion is not well established, neither is the limiting free energy barrier of the process. It had been thought, on the basis of phenomenological calculations, that the free energy to form the initial stalk was so large that its formation could well be the

Submitted September 28, 2006, and accepted for publication December 4, 2006.

Address reprint requests to M. Schick, E-mail: schick@phys.washington.edu.

0006-3495/07/06/3938/11 $2.00

doi: 10.1529/biophysj.106.097063

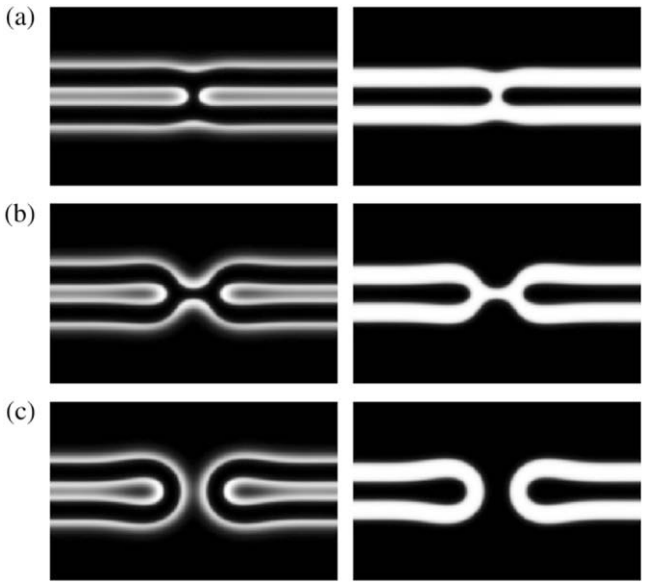

FIGURE 1 The standard stalk model description of membrane fusion. Light regions indicate the areas of headgroups of the bilayer in the left-hand panel, and of tail groups in the right-hand panel. (*a*) Stalk; (*b*) hemifusion diaphragm; and (*c*) fusion pore.

barrier to fusion. Improvements in the way the stalk was modeled (15), and in the phenomenological free energy describing the elastic properties of the membrane (16), which forms the stalk, resulted in a marked reduction in the estimate of the free energy of formation of the stalk. For a bilayer with symmetric leaves characterized by a spontaneous curvature appropriate to dioleoylphosphatidylcholine (DOPC), this quantity is estimated by Kozlovsky and Kozlov (16) to be 43 k_BT, and by Kuzmin et al. (11) to be ~25 k_BT. In contrast to phenomenological theories, self-consistent field theory has been applied to a coarse-grained microscopic model of a symmetric membrane (17), resulting in an even lower estimate of 13 k_BT. Irrespective of the particular number, it would not appear that the formation of the stalk presents the largest barrier to fusion.

If stalk formation is not the rate-limiting process in fusion, what is? In the standard picture in which the stalk expands radially into a hemifusion diaphragm, it is the formation of this structure, which takes a great deal of energy. For a symmetric bilayer of DOPC, a diaphragm of modest radius of 2.5 nm costs on the order of 80 k_BT, if one uses the estimate of Kozlovsky and Kozlov (16) for the diaphragm line tension. How large the diaphragm must become before a pore forms is not clear from this calculation. Kuzmin et al. (11) consider a modified stalk and a different radial symmetric intermediate, a pre-pore. They find its energy, ~60 k_BT, to be less than that of a hemifusion diaphragm, and the largest along the fusion pathway. Self-consistent field calculations examined both the classical pathway (17) and the first stalk-hole mechanism (13), and located the barriers to fusion for symmetric bilayers. In the former, the largest barrier occurred when the hemifusion diaphragm expanded to a radius, which was of the same order of the hydrophobic thickness of a bilayer. Pore formation followed. The value of the barrier ranged from ~25–65 k_BT, depending upon the tension and the architecture of the amphiphiles. The barrier decreases with increasing tension and as the architecture tends toward dioleoylphosphatidylethanolamine (DOPE), and away from DOPC. Calculated barriers in the stalk-hole mechanism tended to be somewhat smaller than in the standard mechanism, but only by a few k_BT. Thus, the two mechanisms seem to be comparable in terms of their energetics, at least for the symmetric membranes examined.

Biological membranes are not symmetric, however. In human red blood cell membranes, for example, most of the cholinephospholipids, sphingomyelin (SM) and phosphatidylcholine (PC), are found in the outer, ectoplasmic, leaf, and most of the aminophospholipids, phosphatidylethanolamine (PE) and phosphatidylserine (PS), are found in the inner, cytoplasmic, leaf (18,19). In particular the mol % of PC in the outer/inner leaf is 22:8, of SM is 20:5, of PS is 0:10, and of PE is 8:27 (18). To maintain this imbalance costs energy (20), therefore it is reasonable to assume that it plays some physiological function. One suggestion is that this imbalance promotes fusion in intracellular events (21–23). The reasoning is as follows. Of the four major lipid groups cited above, three of them, SM, PC, and PS (24) form bilayers under physiological conditions. They make up 65% of the total bilayer, but 84% of the outer, *trans*, leaf. PE, however, does not form lamellae, but rather an inverted hexagonal phase (25). It has often been noted (26) that regions of this nonbilayer phase resemble the nonbilayer configurations posited to occur in fusion. Furthermore, PE resides predominantly in the inner, cytoplasmic, leaf of the plasma membrane. While it makes up only 35% of the total bilayer composition of human red blood cell membranes, it comprises 54% of the inner leaf. It is presumed to also reside predominantly in the outer leaf of a bilayer vesicle within the cell, as the outer leaf of such a vesicle would make contact with the inner leaf of the plasma membrane during fusion of the vesicle and plasma membrane, and thereby have the opportunity to exchange lipid content. However, it is precisely the inner leaf of the plasma membrane and the outer leaf of a vesicle which would be closest to one another during fusion (i.e., would be the *cis* leaves), and would undergo the largest deviation from a planar configuration. Hence, the enhanced concentration of PE in these leaves would presumably promote fusion.

There is much experimental evidence to support the view that the presence of hexagonal-forming lipids in the *cis* leaves enhances fusion. In particular, model membranes (i.e., which have equal composition in both leaves) fuse readily when composed of a mixture of PE and PS approximating that of the inner leaf of the erythrocyte membrane (27), while those consisting of PC and SM do not. Asymmetric

membranes were investigated by Eastman et al. (21), who utilized dioleoylphosphatidic acid (DOPA), a lipid with a headgroup smaller even than PE, which they could move from *cis* to trans layers by applications of a pH gradient. They found fusion to be correlated with the amount of DOPA in the *cis* leaf. With DOPA present in the *cis* leaf in modest amounts, 5 mol %, fusion of large unilamellar vesicles occurred readily on the addition of Ca^{2+}. However, when DOPA was sequestered in the *trans* leaf, little or no fusion was observed. Conversely, if one adds to the *cis* leaf lauroyl lysophosphatidylcholine, which has a large headgroup when compared to its single tail, fusion is inhibited dramatically (23).

As important as this asymmetry appears to be to the process of fusion, it is little addressed in theoretical calculations. In phenomenological ones, it has been accounted for by allowing the inner and outer leaves to be characterized by different spontaneous curvatures. In this way, Kozlovsky and Kozlov (16) predict that the free energy of stalk formation depends essentially only on the spontaneous curvature of the *cis* leaves, and decreases rapidly as this curvature is made more negative, (i.e., as one proceeds from the lamellar formers toward the hexagonal formers). A similar calculation and result follows for the free energy of formation of the hemifusion diaphragm (28). That the free energies of the stalk and hemifusion diaphragm depend essentially only on the properties of the *cis* leaf is in accord with the experimental observations (21). There are no direct results for the effect of the asymmetry on the largest barrier to fusion, however. Further, by treating the entire *cis* layer as having the same spontaneous curvature, the calculation cannot capture the ability of hexagonal-forming lipids to respond locally to an environment in which the leaves are locally deformed, which will result, in general, in their distribution being nonuniform (29). Simulations of fusion have not yet considered the effects of asymmetry, presumably because the asymmetric distribution represents a constrained equilibrium, a situation more difficult to handle than an unconstrained one.

In this article, we consider two important conditions noted above; that the bilayer leaves consist of at least two classes of lipids, lamellar formers and hexagonal formers, and that these lipids are distributed asymmetrically with respect to the *cis* and *trans* layers. We do so by extending the application of self-consistent field theory to microscopic models of membranes initiated earlier (13,17). The basic assumption of this approach is that the self-assembly into bilayer vesicles and the processes which these vesicles can undergo, such as fusion, are common to systems of amphiphiles, of which lipids are but one example. Recent work on vesicles consisting of diblock copolymers serves to illustrate this point (30). It follows that these processes can be explored in whatever system of amphiphiles proves to be most convenient. For the application of self-consistent field theory, that system is one of block copolymers in a homopolymer solvent. While the processes that amphiphiles undergo are presumably universal, the energy scales of these processes are system-dependent, and thus it is necessary to be able to compare the energy scale in a biological bilayer with the scale in a system of block copolymers. From the comparison of the value of a dimensionless ratio in the former system to the same ratio calculated in the latter, it was determined that the energies in the biological system were greater than those in the polymer system by a factor of $\sim$2.5. The ratio chosen for comparison was that of two energies, the thermal energy, k_BT, and the surface free energy per unit area of the bilayer multiplied by the square of its thickness.

We examine in two stages the effect on the energies of fusion intermediates caused by the asymmetric distribution of amphiphiles in multicomponent bilayers. First, we consider the effect on the barriers to fusion due to the presence of two kinds of amphiphiles in leaves of identical composition, as in artificial membranes. We do this for the standard mechanism, and for both the first and second stalk-hole fusion mechanisms. We find that the barriers are reduced appreciably because the hexagonal-forming amphiphiles can go to the regions where they relieve the most strain (29). The barriers in the two variants of the stalk-hole mechanism are not very different from one another. We then consider the same overall composition, but redistribute the two amphiphiles asymmetrically, with the hexagonal formers being more concentrated in the *cis* leaves. The barriers in the standard fusion mechanism and in the second stalk-hole mechanism are calculated. The overall effect of having two such different amphiphiles distributed unequally between the two leaves is dramatic. The major barriers to fusion in the two scenarios are reduced to such an extent that they are now comparable to the rather small initial barrier to stalk formation. This barrier is not affected appreciably by the addition of the hexagonal formers nor by their asymmetric distribution, and remains on the order of 13 k_BT. As a result, the fusion pathway consists of two small barriers. Once bilayers are brought sufficiently close to initiate the process, fusion should therefore proceed rapidly.

THE MODEL

The model is similar to that employed earlier (13,17), so we will only discuss here the necessary extensions. We consider a system of two different amphiphiles, which are each AB block copolymers and are denoted 1 and 2, and a solvent of A homopolymer. The volumes occupied by a solvent chain of N segments, and of a chain of amphiphile 1, also taken to be of N segments, are Nv, where v is the volume of each segment. The volume occupied by a chain of amphiphile 2 of $\tilde{\alpha}N$ segments is $\tilde{\alpha}Nv$. The fraction of hydrophilic, A, monomers in amphiphile 1 is f_1 and that in amphiphile 2 is f_2. In our subsequent calculations we shall take $f_1 = 0.4$, close to the value of 0.43 which would characterize DOPC, and $f_2 = 0.294$, approximately the value characterizing DOPE (17). In

order that the hydrophobic length of the two different amphiphiles be the same, we require $(1-f_1)Nv = (1-f_2)\tilde{\alpha}Nv$ so that $\tilde{\alpha} = 0.85$. Thus we have two amphiphiles with the same hydrophobic length, but different hydrophilic lengths. Amphiphile 2 is a hexagonal former with a smaller hydrophilic headgroup than amphiphile 1, which is a lamellar former. We denote the local volume fraction of hydrophilic elements of amphiphile 1 to be $\phi_{A,1}(\mathbf{r})$, of amphiphile 2 to be $\phi_{A,2}(\mathbf{r})$, and of the solvent to be $\phi_{A,s}(\mathbf{r})$. The total local volume fraction of hydrophilic elements is denoted

$$\phi_A(\mathbf{r}) = \phi_{A,1}(\mathbf{r}) + \phi_{A,2}(\mathbf{r}) + \phi_{A,s}(\mathbf{r}). \tag{1}$$

Similarly the total local volume fraction of hydrophobic elements is

$$\phi_B(\mathbf{r}) = \phi_{B,1}(\mathbf{r}) + \phi_{B,2}(\mathbf{r}). \tag{2}$$

The amounts of each of the components are controlled by activities, ζ_1, ζ_2, and ζ_s. The system is taken to be incompressible and of volume V. Because of the incompressibility constraint, only two of the activities are independent. Within the self-consistent field approximation, the excess free energy, $\delta\Omega^{sym}(T, A, \zeta_1, \zeta_2, \zeta_s)$, of the bilayer system of area A, is given by

$$\begin{aligned}\frac{Nv}{k_BT}\delta\Omega^{sym} = &-\zeta_1 Q_1 - \zeta_2 Q_2 - \zeta_s Q_s + \int d\mathbf{r}[\chi N\phi_A(\mathbf{r})\phi_B(\mathbf{r}) \\ &- w_A(\mathbf{r})\phi_A(\mathbf{r}) - w_B(\mathbf{r})\phi_B(\mathbf{r}) \\ &- \xi(\mathbf{r})(1-\phi_A(\mathbf{r})-\phi_B(\mathbf{r}))],\end{aligned} \tag{3}$$

where $Q_1(T, [w_A, w_B])$, $Q_2(T, [w_A, w_B])$, and $Q_s(T, [w_A])$ are the configurational parts of the single chain partition functions of amphiphiles 1 and 2 and of solvent. They have the dimensions of volume, and are functions of the temperature, T, which is inversely related to the Flory interaction χ, and functionals of the fields w_A and w_B. These fields, and the Lagrange multiplier $\xi(\mathbf{r})$, which enforces the local incompressibility condition, are determined by the self-consistent equations

$$w_A(\mathbf{r}) = \chi N\phi_B(\mathbf{r}) + \xi(\mathbf{r}), \tag{4}$$

$$w_B(\mathbf{r}) = \chi N\phi_A(\mathbf{r}) + \xi(\mathbf{r}), \tag{5}$$

$$1 = \phi_A(\mathbf{r}) + \phi_B(\mathbf{r}), \tag{6}$$

$$\phi_A(\mathbf{r}) = -\zeta_1\frac{\delta Q_1[w_A, w_B]}{\delta w_A(\mathbf{r})} - \zeta_2\frac{\delta Q_2[w_A, w_B]}{\delta w_A(\mathbf{r})} - \zeta_s\frac{\delta Q_s[w_A]}{\delta w_A(\mathbf{r})}, \tag{7}$$

$$\phi_B(\mathbf{r}) = -\zeta_1\frac{\delta Q_1[w_A, w_B]}{\delta w_B(\mathbf{r})} - \zeta_2\frac{\delta Q_2[w_A, w_B]}{\delta w_B(\mathbf{r})}. \tag{8}$$

The partition functions are obtained from the solution of a modified diffusion equation, as detailed in the first article in this series (17), and the barriers to fusion are calculated for the standard and for the stalk-hole mechanisms as in the previous two articles (13,17). The free energy in the self-consistent field approximation, $\delta\Omega^{sym}_{scf}$, is obtained by inserting into the free energy of Eq. 3 the functions satisfying the self-consistent Eqs. 4–8 with the result

$$\begin{aligned}\frac{Nv}{k_BT}\delta\Omega^{sym}_{scf}(T, A, \zeta_1, \zeta_2, \zeta_s) = &-\zeta_1 Q_1(T, [w_A, w_B]) \\ &- \zeta_2 Q_2(T, [w_A, w_B]) - \zeta_s Q_s(T, [w_A]) \\ &- \int d\mathbf{r}\chi N\phi_A(\mathbf{r})\phi_B(\mathbf{r}),\end{aligned} \tag{9}$$

where we have set $\int \xi(\mathbf{r})d\mathbf{r} = 0$. With the excess free energy known, the surface free energy per unit area, or equivalently, the surface tension, γ, follows from

$$\gamma(T, \zeta_1, \zeta_2, \zeta_s) \equiv \lim_{A\to\infty}\frac{\delta\Omega(T, A, \zeta_1, \zeta_2, \zeta_s)}{A}. \tag{10}$$

Calculation of the barrier to fusion in the standard mechanism is relatively straightforward because all intermediates, the stalk, hemifusion diaphragm, and pore, are characterized by axial symmetry about the z axis, and reflection symmetry in the xy plane. The former symmetry is absent in the intermediates of the stalk-hole mechanisms. To make tractable the calculation of the barrier along this path, the actual intermediates were approximated by intermediates constructed from segments of configurations which possessed both symmetries and whose free energies, therefore, were easily obtained (13).

Just before formation of the stalk-hole complex, the elongated stalk was treated as if it were in the shape of a circular arc with a fractional angle, $0 \le \alpha \le 1$, and radius R, as shown schematically in Fig. 2 *a*. Its free energy is

$$F_1(R, \alpha) = \alpha F_{IMI}(R) + F_s, \tag{11}$$

where F_{IMI} is the energy of the structure shown at the extreme right of Fig. 2 *a*, which corresponds to $\alpha = 1$, and F_s is the free energy of a stalk. This is because it is the sum of the energies of the two end caps of a structure for which $\alpha \neq 1$, and these two end caps together make a stalk.

Just after formation of the stalk-hole complex in the first stalk-hole mechanism, there is a hole in one of the two bilayers (31–35), which is partially surrounded by the elongated stalk. This intermediate is approximated by the configuration shown in Fig. 2 *b* whose free energy is

$$F_2(R, \alpha) = \alpha F_{HI}(R) + (1-\alpha)F_H(R-\delta) + F_d. \tag{12}$$

Here F_{HI} is the free energy of the structure with $\alpha = 1$ in which the stalk would have completely surrounded the hole forming a hemifusion intermediate, $F_H(R-\delta)$ is the free energy of a hole of radius $R-\delta$ in a bilayer, and F_d is the free energy of the defects at the end of the arc. Equality of the free energies of Eqs. 11 and 12 defines a ridge line in the space of parameters α and R, and the minimum of this ridge defines a saddle point along this fusion path.

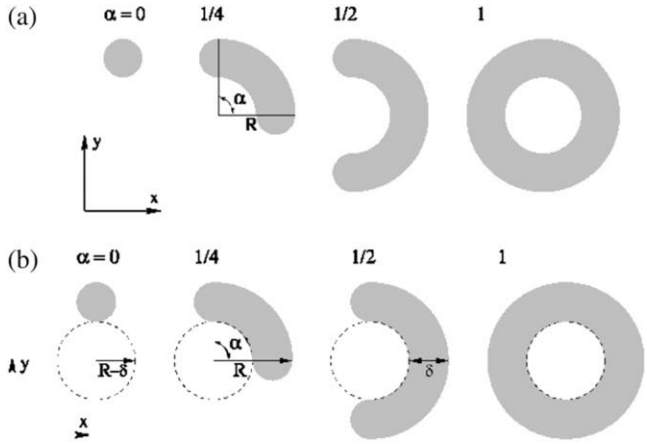

FIGURE 2 (*a*) Parameterization of the elongated stalk. The shading schematically shows the location of the hydrophobic segments in the plane of symmetry between fusing bilayers. The arc radius R corresponds to the radial distance to the outer hydrophilic/hydrophobic interface in the plane of symmetry. Values of the fractional arc angle, α, defined in the range [0,1], are given at the top of each stalk configuration. Note that $\alpha = 0$ corresponds to the original stalk configuration. (*b*) Parameterization of the stalk-hole complex. In the first stalk-hole mechanism, there is a hole in one bilayer and the projection of its edge is shown with a dashed line. In the second stalk-hole mechanism, there is a hole in each of the bilayers, and the dashed line represents the projection of their edges. The radius of the hole, or holes, is $R-\delta$. The hydrophobic thickness of the bilayer is δ. Values of the fractional arc angle, α, defined in the range [0,1], are given at the top of each configuration.

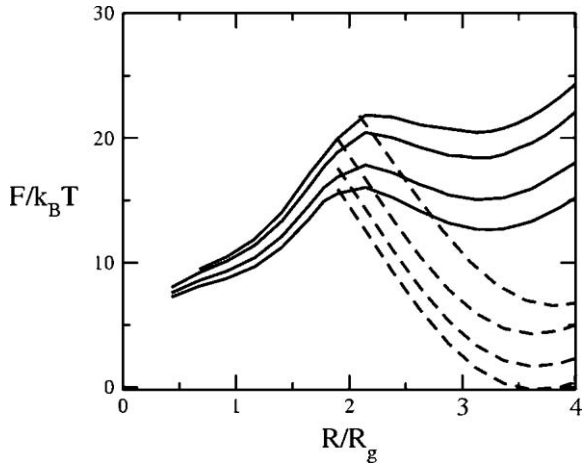

FIGURE 3 Excess free energies of fusion intermediates in the standard model are shown at a tension of $\gamma/\gamma_0 = 0.1$. Solid curves indicate stalk/hemifusion intermediates and dashed curves fusion pores. The bilayers consist of AB diblocks of two different lengths and architectures. The first diblock is described by N segments and $f_1 = 0.4$, and the second diblock by $\tilde{\alpha}N$ segments with $\tilde{\alpha}_2 = 0.85$ and $\tilde{\alpha}_2(1-f_2) = 0.6$. From top to bottom, the volume fractions of type 2 diblocks in the bilayers are 0.00, 0.04, 0.11, and 0.17.

In the second stalk-hole mechanism, just after formation of the stalk-hole complex, there are two holes, one in each bilayer, partially surrounded by the elongated stalk. Again, the picture is as in Fig. 2 *b*, but now the circular object in the center of the figure represents the two holes, rather than the one as previously. Thus, the figure at the extreme right now represents a fusion pore. The free energy of this configuration is

$$F_3(R,\alpha) = \alpha F_{\text{pore}}(R) + (1-\alpha)F_{2\text{H}}(R-\delta) + F'_{\text{d}}. \quad (13)$$

Here $F_{\text{pore}}(R)$ is the free energy of a pore of radius R, $F_{2\text{H}}(R-\delta) = 2F_{\text{H}}(R-\delta)$ is the free energy of two holes, each of radius $R-\delta$, one above the other, and F'_{d} the energy of the two defects at the end of the arc. Again equality of Eqs. 11 and 13 defines a ridge line in the space of parameters α and R. The minimum along this ridge defines the fusion barrier along this second stalk-hole pathway.

RESULTS FOR SYMMETRIC BILAYERS

We first show in Fig. 3 how the addition of the hexagonal-forming amphiphiles affects the barrier to fusion in the standard mechanism. We plot there in solid lines the free energy of the stalk, which expands into a hemifusion diaphragm as a function of the structure's radius divided by the radius of gyration, R_{g}, of the larger amphiphile. (The hydrophobic thickness of a single bilayer composed of amphiphiles with $f = 0.4$ is 2.7 R_{g}.) When the radius is smaller than $\sim$0.5 R_{g}, we find no stable stalk solution of the self-consistent equations. We have taken the volume Nv which appears in the free energy, Eq. 9, to be $Nv = 1.54R_{\text{g}}^3$, as in our previous work (13,17). The four solid curves in Fig. 3 correspond to volume fractions of the hexagonal former of 0, 0.04, 0.11, and 0.17 from top to bottom. The first thing to be noted is that, at small radii, there are no solutions that show a local minimum of the free energy as a function of radius. Such solutions would correspond to a metastable stalk. That there are no metastable stalks in a bilayer composed of amphiphiles with $f = 0.4$, close to the value $f = 0.43$, which would characterize DOPC, had been noted earlier (17). One consequence of this observation is that fusion of such bilayers would have to take place via one large thermal excitation due to the lack of a metastable stalk intermediate. As a consequence, the timescale for fusion would be expected to be rather long, certainly longer than if the intermediate were metastable. The results of Fig. 3 show that the addition of hexagonal formers up to volume fractions of 0.17 equally in each leaf does not bring about the existence of a metastable stalk.

The free energies of fusion pores for the same volume fractions of hexagonal formers are shown in dotted curves. We take the barrier to fusion to be that value at which the free energies of a hemifusion diaphragm and fusion pore of the same radius are equal. The bilayer is under a tension of $\gamma/\gamma_0 = 0.1$, where γ_0 is the interfacial free energy per unit

area between coexisting solutions of hydrophobic and hydrophilic homopolymers at the same temperature. At larger values of the radius of the hemifusion diaphragm than shown in the figure, the free energy of the diaphragm decreases due to the tension. One sees from Fig. 3 that the barrier to fusion does indeed decrease with the addition of hexagonal formers. As can be seen in the figure, this reduction comes about both because of the reduction in energy of the fusion pore and of the hemifusion diaphragm. The reduction in the pore energy is due to the effect of the hexagonal formers, which can go to the sharp bend of the *cis* leaf existing in the pore. Similarly, the reduction in the energy of the hemifusion diaphragm is due to the hexagonal formers concentrating at the rim of the diaphragm. This is shown in Fig. 4. In Fig. 4 *a*, the volume fractions of the heads (*dashed line*), and tails (*solid line*) of the hexagonal-forming amphiphile far from the hemifusion diaphragm are shown as a function of z/R_g. In Fig. 4 *b*, we show the volume fractions of the hexagonal-forming amphiphile in a cut through the hemifusion diaphragm itself in the plane of reflection symmetry, the $z = 0$ plane, as a function of the radial coordinate, ρ/R_g. (Recall that such a hemifusion diaphragm is shown in Fig. 1 *b*.) One sees that the diaphragm has an approximate radius of 5 R_g. A comparison of the plots in Fig. 1, *a* and *b*, shows that the local volume fraction of tails of the hexagonal former at the diaphragm rim increases by ~20%, and that the local density of heads of this amphiphile increases there by almost 50%.

The barrier to fusion in the standard mechanism is shown in the upper curve of Fig. 5 as a function of concentration of the hexagonal-forming amphiphile. One sees that the dependence is nonlinear. The effect of the hexagonal-forming amphiphile in reducing the barrier to fusion is greatest when this amphiphile is first added, as it can go to the region where it relieves the most strain. As more and more is added, its ability to reduce the barrier to fusion is lessened.

The barrier to fusion in the first stalk-hole mechanism is shown in the lower curve. We have assumed a reasonable energy of 4 k_BT for the defects that appear at the end of the elongated stalk partially surrounding a hole in one of the bilayers. That the barrier to fusion is somewhat lower in the first stalk-hole mechanism than in the standard one, and is much less sensitive to the architecture than is the standard mechanism for a system composed primarily of amphiphile characterized by $f = 0.4$ could have been anticipated by the results presented in Fig. 10 of Katsov et al. (13). As seen there, for $f = 0.35$, and $\gamma/\gamma_0 = 0.1$, the barrier to fusion is somewhat lower in the first stalk-hole mechanism than in the standard mechanism, and the barrier in the latter varies more rapidly with architecture, f, than in the stalk-hole mechanism.

In the upper panel of Fig. 6, we compare the fusion barriers in the first and second stalk mechanisms. The former is shown in solid circles and the latter is shown in solid

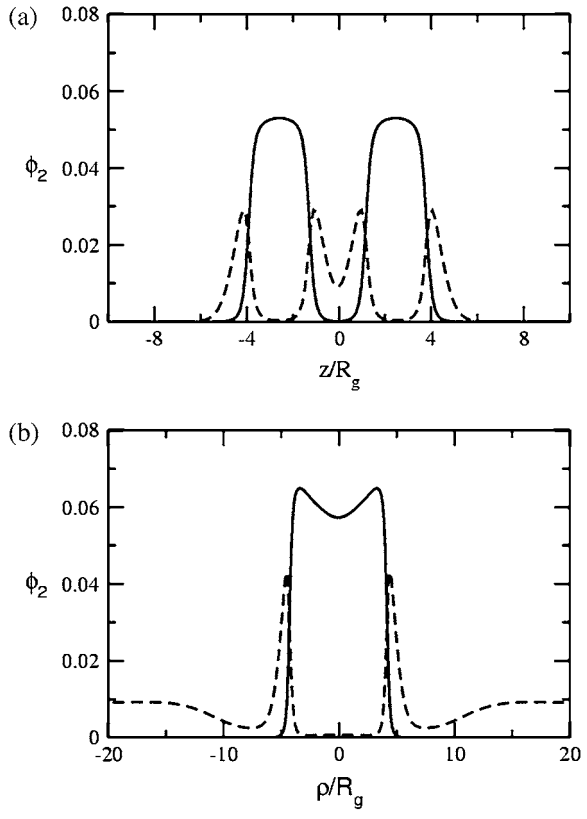

FIGURE 4 (*a*) Volume fractions, ϕ_2, of the headgroup, dashed line, and tail, solid line, of the hexagonal-forming amphiphile in the bilayers far from the hemifusion diaphragm are shown in a cut perpendicular to the bilayers as a function of the dimensionless vertical coordinate z/R_g. (*b*) These same volume fractions are shown in the $z = 0$ plane of symmetry, which passes through the hemifusion diaphragm itself as a function of the dimensionless radial coordinate ρ/R_g. The hemifusion diaphragm has a radius of ~5 R_g.

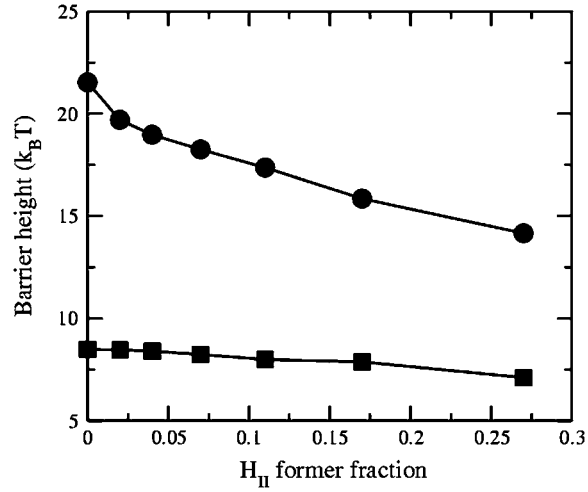

FIGURE 5 Barrier height of fusion process as a function of the volume fraction of the hexagonal-forming (H_{II}) amphiphile. The upper curve shows the barrier heights in the standard stalk-hemifusion mechanism. The lower curve shows the barrier heights in the first stalk-hole mechanism with a defect energy of $F_d = 4\ k_BT$.

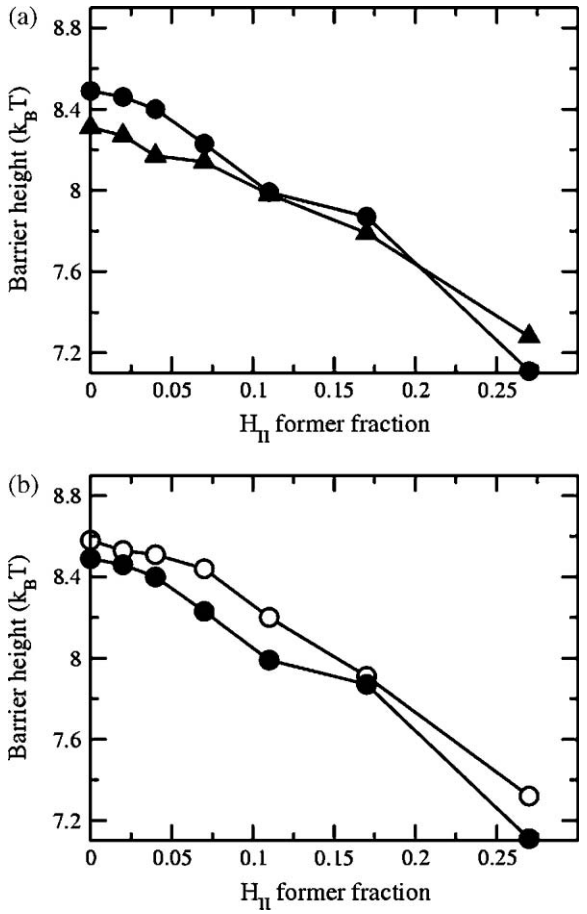

FIGURE 6 (*a*) Comparison of the barrier to fusion in the first (*solid circles*) and second (*solid triangles*) stalk-hole mechanisms as a function of volume fraction of hexagonal-forming (H_{II}) amphiphile. (*b*) Comparison of barrier to fusion in the first stalk-hole mechanism with defect energy of 4 k_BT (*open circles*) and vanishing defect energy (*solid circles*).

triangles. Defect energies are taken to be 4 k_BT. One sees that there is not a great deal of difference in the energy barriers in the two mechanisms. One also notes that the second stalk-hole mechanism has a lower energy than that of the first when the fraction of hexagonal-forming amphiphiles is low. The situation is reversed as the fraction increases. This is to be expected as the second stalk-hole intermediate consists of portions of a fusion pore and of two holes. Both of these structures are disfavored by the hexagonal-forming amphiphiles. On the other hand, the first stalk-hole intermediate consists of portions of a hemifusion diaphragm, and only one hole. The hemifusion diaphragm is favored by the hexagonal-forming amphiphiles.

The lower panel of Fig. 6 illustrates that the barrier to fusion in the stalk-hole mechanism is not very sensitive to the choice of defect energy. The barrier heights are shown there for the first stalk-hole mechanism for the case in which the defect energy is 4 k_BT (*open circles*) and in which the defect energy vanishes (*solid circles*).

RESULTS FOR ASYMMETRIC BILAYERS

We now consider the situation in which the compositions of the two different leaves of the bilayer differ. In particular, we will fix the composition of the hexagonal-forming lipid in the *cis* leaf. The overall composition of lamellar- and hexagonal-forming amphiphiles in the bilayer is still controlled by the activities ζ_1, ζ_2, and ζ_s and the incompressibility condition. Therefore we want to calculate the excess free energy $\delta\Omega^{\text{asym}}(T, A, \zeta_1, \zeta_2, \zeta_s, n_2^{\text{cis}})$, where n_2^{cis} is the number of hexagonal-forming amphiphiles in the *cis* leaf of the bilayer:

$$n_2^{\text{cis}} = \frac{1}{\alpha N v}\int d\mathbf{r}\phi_2(\mathbf{r}) = \frac{1}{\alpha N v f_2}\int d\mathbf{r}\phi_{A,2}(\mathbf{r}). \qquad (14)$$

The integral is over the volume of the *cis* leaf of the bilayer. In the second equality, we determine the number of hexagonal formers in the *cis* layer by counting the number of their headgroups, which will be more convenient. Rather than calculate the free energy in an ensemble in which the number of hexagonal-forming lipid heads is fixed, it is far easier, as usual, to calculate the free energy in an ensemble in which a local field, $h(\mathbf{r})$, controls the average local average value of $\phi_{A,2}(\mathbf{r})$, and therefore of n_2^{cis}. This adds to the system's internal energy a term of the form

$$-\frac{k_BT}{Nv}\int d\mathbf{r}h(\mathbf{r})\phi_{A,2}(\mathbf{r}). \qquad (15)$$

The field $h(\mathbf{r})$ is taken to be non-zero only in the *cis* leaf. Our choice is

$$h(\mathbf{r}) = h(z,\rho) = h_0 \quad |z| \le 0.6R_g \quad \text{and} \quad \rho \ge R + 0.6R_g, \\ = 0 \quad \text{otherwise}, \qquad (16)$$

with R the radius of the hemifusion diaphragm defined previously (17). The field is non-zero only in the region shown in Fig. 7. From the coupling term of Eq. 15, one sees that the greater the strength of the field, h_0, the larger will be the volume fraction of the hexagonal formers in the *cis* layer. Once the excess free energy of this asymmetric system, $\delta\tilde{\Omega}^{\text{asym}}(T, A, \zeta_1, \zeta_2, \zeta_s, h_0)$, is obtained, differentiation of it

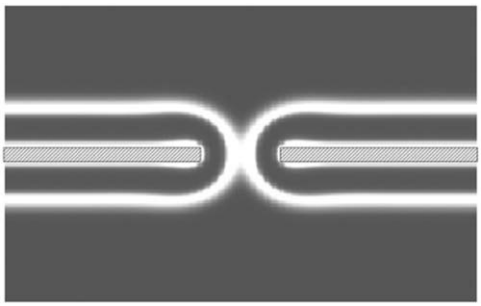

FIGURE 7 Density profile of a fusion pore. The region where external fields are applied to maintain asymmetry is marked by shaded areas on the density plot of small headgroups. White regions indicate the areas where small headgroups are concentrated and the gray regions the areas in which their concentration is strongly reduced.

with respect to the field strength h_0 yields $\phi_{A,2}(\mathbf{r})$. The number of hexagonal formers in the *cis* layer, $n_2^{cis}(T, A, \zeta_1, \zeta_2, \zeta_s, h_0)$, is then obtained by integration of this quantity, Eq. 14. The value of the field strength h_0 can then be adjusted to obtain the desired concentration of hexagonal formers in the *cis* layer.

The excess free energy is obtained by a simple extension of the procedure employed to determine that of the symmetric bilayer. We obtain $\delta\tilde{\Omega}^{asym}(T, A, \zeta_1, \zeta_2, \zeta_s, h_0)$,

$$\frac{Nv}{k_E T}\delta\tilde{\Omega}^{asym} = -\zeta_1 Q_1(T,[w_A, w_B]) - \zeta_2 Q_2(T,[w_A - h, w_B]) - \zeta_s Q_s(T,[w_A]) + \int d\mathbf{r}[\chi N\phi_A(\mathbf{r})\phi_B(\mathbf{r}) - w_A(\mathbf{r})\phi_A(\mathbf{r}) - w_B(\mathbf{r})\phi_B(\mathbf{r}) - \xi(\mathbf{r})(1 - \phi_A(\mathbf{r}) - \phi_B(\mathbf{r}))]. \quad (17)$$

The self-consistent equations, Eqs. 4–8, are unaffected. Again, the free energy in the self-consistent field approximation is obtained by substituting the functions that satisfy the self-consistent equations into the free energy of Eq. 17 with the result

$$\frac{Nv}{k_B T}\delta\tilde{\Omega}^{asym}_{scf} = -\zeta_1 Q_1(T,[w_A, w_B]) - \zeta_2 Q_2(T,[w_A - h, w_B]) - \zeta_s Q_s(T,[w_A]) - \int d\mathbf{r}\chi N\phi_A(\mathbf{r})\phi_B(\mathbf{r}). \quad (18)$$

The desired free energy, $\delta\Omega^{asym}_{scf}(T, A, \zeta_1, \zeta_2, \zeta_s, n_2^{cis})$, is now obtained by a Legendre transform

$$\frac{Nv}{k_B T}\delta\Omega^{asym}_{scf}(T,A,\zeta_1,\zeta_2,\zeta_s,n_2^{cis}) = \frac{Nv}{k_B T}\delta\tilde{\Omega}^{asym}_{scf}(T,A,\zeta_1,\zeta_2,\zeta_s,h_0) + \int d\mathbf{r}h(\mathbf{r})\phi_{A,2}(\mathbf{r}), \quad (19)$$

so that

$$\frac{Nv}{k_B T}\delta\Omega^{asym}_{scf} = -\zeta_1 Q_1(T,[w_A, w_B]) - \zeta_2 Q_2(T,[w_A - h, w_B]) - \zeta_s Q_s(T,[w_A]) + \int d\mathbf{r}[h(\mathbf{r})\phi_{A,2}(\mathbf{r}) - \chi N\phi_A(\mathbf{r})\phi_B(\mathbf{r})]. \quad (20)$$

Because the system is constrained to have a different concentration of hexagonal formers in the *cis* leaf than in the *trans* leaf, its free energy will clearly be greater than if it were not so constrained. This is also true of the free energies of the various intermediates, like the stalk, hemifusion diaphragm, and pore. For the fusion process, however, we are interested in differences in free energies between the intermediates and the flat bilayers, and these differences can certainly be less in the constrained system.

Standard mechanism

The calculations for the standard mechanism are relatively straightforward due to the axial and reflection symmetry of the stalk, the hemifusion diaphragm, and the pore.

In Fig. 8 we show results for a bilayer under a tension $\gamma/\gamma_0 = 0.1$ composed of the lamellar-former comprising a fraction $\phi_1 = 0.650$ of the bilayer by volume, and the hexagonal former comprising a fraction $\phi_2 = 0.350$ by volume. Results are presented for the excess free energy of the hemifusion diaphragm (*solid lines*) and of the fusion pores (*dashed lines*) for different volume fractions in the *cis* leaf of the hexagonal-forming amphiphile. In the upper set of curves, there is no asymmetry, so that the volume fraction of hexagonal former in the *cis* leaf, $\phi_2^{cis} = 0.350$, is the same as in the whole bilayer. In the middle curve, the volume fraction of the hexagonal-former in the *cis* leaf has been increased to $\phi_2^{cis} = 0.395$. Its volume fraction in the *trans* leaf is concomitantly reduced to $\phi_2^{trans} = 0.305$, and the volume fractions of the lamellar former in the *cis* and *trans* leaves are 0.605 and 0.695, respectively. In the lowest curve, we have set $\phi_2^{cis} = 0.431$, so that $\phi_2^{trans} = 0.269$, and the volume fractions of the lamellar former in the *cis* and *trans* leaves are 0.569 and 0.731. The barrier to fusion is reduced from 11 $k_B T$ to 8.5 $k_B T$, to 5 $k_B T$, as the asymmetry increases. For the largest asymmetry shown, the barrier to fusion is essentially no greater than the barrier to formation of the initial stalk itself. Furthermore for this asymmetry, the intermediate stalk is finally a metastable structure. As noted earlier, this has a large effect on the timescale of fusion by permitting the process to occur in two stages rather than one.

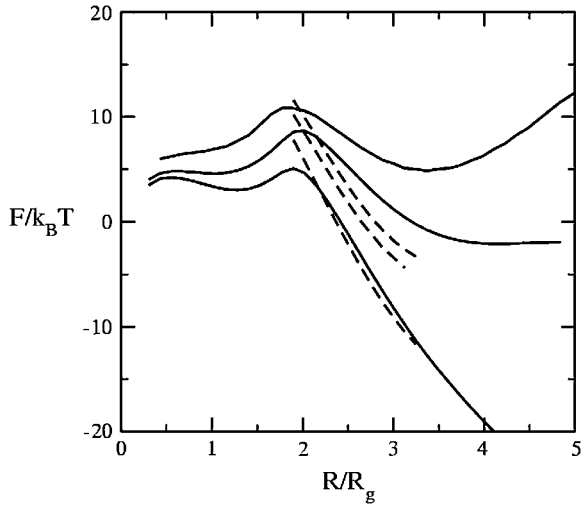

FIGURE 8 Excess free energies of standard fusion intermediates for bilayers of the same overall composition, but with varying transbilayer distributions under $\gamma/\gamma_0 = 0.1$ tension. The bilayers here contain 65% lamellar-forming diblock and 35% hexagonal-forming diblock. The solid curves represent excess free energies of stalk/hemifusion diaphragm and the dashed curves excess free energies of fusion pores. In the upper set of curves, there is no asymmetry, so that the volume fraction of hexagonal former in the *cis* leaf, $\phi_2^{cis} = 0.350$, is the same as in the whole bilayer. In the middle curve, the volume fraction of the hexagonal former in the *cis* leaf, has been increased to $\phi_2^{cis} = 0.395$. In the lowest curve, we have set $\phi_2^{cis} = 0.431$. The barrier to fusion is reduced from 11 $k_B T$ to 8.5 $k_B T$, to 5 $k_B T$ as the asymmetry increases.

Stalk-hole mechanism

We have calculated the barrier to fusion between asymmetric bilayers in the second stalk-hole mechanism. We have chosen this path, rather than the first stalk-hole mechanism, because the latter involves the calculation of the free energy of a hole in an asymmetric bilayer, and of a hemifusion diaphragm, which consists of the *cis* and *trans* layer of one of the original bilayers. As the bilayer is not symmetric, neither is the hemifusion diaphragm, and this lack of symmetry about the x, y plane makes the calculation rather slow. The second stalk-hole mechanism does not involve this asymmetric hemifusion diaphragm, although it still involves holes in asymmetric bilayers. The calculation of the energies in this pathway is more rapid. We have already shown that there is not a great deal of difference in the barrier energies in the two pathways in symmetric bilayers, Fig. 6 *a*, and assume that the same is true with asymmetric bilayers. If anything, we will overestimate the fusion barrier of the stalk-hole mechanism because, as we add hexagonal formers, the barrier in the second stalk-hole pathway we calculate will probably become somewhat larger than that in the first pathway, just as it is in the symmetric bilayer case, Fig. 6 *a*.

Our results for the barrier to fusion of asymmetric bilayers within the second stalk-hole mechanism are shown in Fig. 9. We have calculated them for bilayers in which the average volume fraction of hexagonal formers in the entire bilayer is kept fixed at $\phi_2 = 0.350$, while the fraction of hexagonal formers in the *cis* layer, ϕ_2^{cis}, takes the values $\phi_2^{\text{cis}} = 0.350$ (i.e., no asymmetry), $\phi_2^{\text{cis}} = 0.395$, and $\phi_2^{\text{cis}} = 0.431$. The barrier to fusion for this second stalk-hole pathway is shown by the triangles. The values of α at the saddle point in the fusion pathway are $\alpha = 0.073$ for $\phi_2^{\text{cis}} = 0.350$, $\alpha = 0.174$ when $\phi_2^{\text{cis}} = 0.395$, and $\alpha = 0.18$ when $\phi_2^{\text{cis}} = 0.431$. These barriers to fusion are compared to those calculated in the standard mechanism and shown in squares. These values were shown previously in Fig. 8. Finally, we also compare them with the free energies of the stalk, shown in circles.

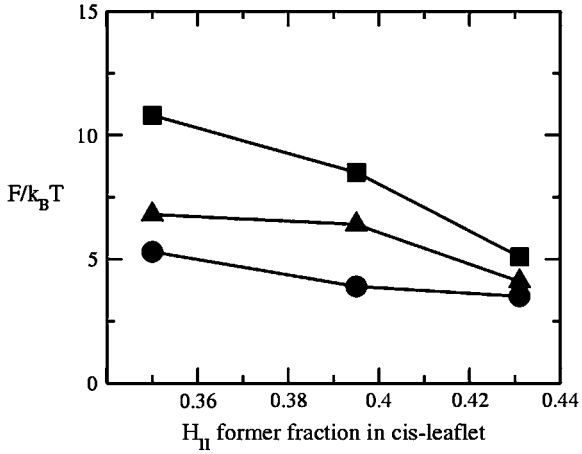

FIGURE 9 Comparison of the barrier to fusion of asymmetric bilayers containing an average volume fraction of hexagonal formers of $\phi_2 = 0.35$ as calculated along the standard pathway (*squares*) and the second stalk-hole pathway (*triangles*) for three different volume fractions of hexagonal formers in the *cis* layer; $\phi_2^{\text{cis}} = 0.350, 0.395, 0.431$. Also shown is the free energy of a stalk (*circles*) in the same systems.

We note that the small values of α in the stalk-hole mechanism imply that the stalk does not have to elongate very much to nucleate the formation of the two holes which, when surrounded by the stalk, will become the fusion pore. (We recall that in surrounding the holes, the energy of the system is reduced as the line tensions of the bare holes are replaced by the lower line tension of a hole next to a stalk (13).) Hole formation is enhanced, and the barrier to fusion reduced, because the majority amphiphile, $\phi_1 = 0.65$, is a lamellar-former with $f = 0.4$. Furthermore, the actual volume fraction of the lamellar former near the rim of a hole will be larger than this because the amphiphiles are free to move within a leaf to that region where they will reduce the energy most. The increase of α with the fraction of hexagonal formers in the *cis* leaf is readily understood. As the fraction of hexagonal former in the *cis* leaf increases, the energy of a pore decreases, as noted previously. It follows from Eq. 13 that α, the fraction of the stalk-hole intermediate that resembles a pore, will increase.

DISCUSSION

We have employed a model of a mixture of two amphiphiles—one that is a lamellar former, the other a hexagonal former. The ratio of their hydrophilic part to the entire molecule was chosen so that the first resembles DOPC and the latter resembles DOPE. The two have the same hydrophobic, but different hydrophilic, volumes. We have solved the model within self-consistent field theory.

We first considered bilayers whose leaves have identical compositions, and added hexagonal formers to each leaf equally. We examined the effect of this addition on the barrier to fusion as calculated in the standard mechanism, and the first and second stalk-hole mechanisms. We noted that the stalk was not a metastable intermediate in these systems in which DOPC-like amphiphiles were the dominant constituent. Nonetheless, we considered the barrier energy and found it to be reduced significantly in the standard mechanism from $\sim$24 k_BT with no hexagonal-formers to $\sim$11 k_BT with a volume fraction of 0.35 hexagonal formers. This is seen in Figs. 5 and 9. As noted earlier (17), we expect that the energies in biological, lipid, membranes are higher by a factor of $\sim$2.5 than in the block copolymer membranes we are considering. Thus the above barrier values would correspond to one of 60 k_BT being reduced to 28 k_BT. The reduction in the fusion barrier of the standard mechanism is due to a reduction in the energy of the hemifusion intermediate, partly because the average number of hexagonal formers has increased (16), and partly because the hexagonal-forming amphiphiles preferentially go to the edge

of the hemifusion diaphragm, as seen in Fig. 4. Fig. 5 shows that the greatest rate of decrease comes about when the hexagonal formers are first added to the pure bilayer of lamellar formers. This rapid decrease occurs because the hexagonal formers go to the regions where they can most readily reduce the free energy. The distribution of the different amphiphiles is not spatially uniform when there are fusion intermediates. The reduction of the barrier energy in the stalk-hole mechanism is more modest, but is not insignificant. In the second stalk-hole mechanism, it is reduced from 8.3 k_BT when there are no hexagonal-formers to 6.8 k_BT with a volume fraction of 0.350 hexagonal-formers. Again this would correspond to a reduction from 21 k_BT to 17 k_BT in a biological system.

We then examined the effect on the barrier to fusion of an unequal distribution of hexagonal and lamellar formers in the two leaves. We considered a system in which the hexagonal formers make up a volume fraction of 0.350 of the whole system, much as they do in human red blood cell membranes. This brings about a further significant reduction in the barrier to fusion in both mechanisms. In the standard mechanism, this is due to the reduction in energy of the hemifusion diaphragm, while in the stalk-hole mechanism it is due primarily to the reduction in energy of the elongated stalk.

The energy of the initial stalk itself is not affected very much either by the addition of hexagonal formers to each leaf equally, as seen in Fig. 3, or by the redistribution of the hexagonal formers between the two leaves, as seen in Fig. 9. The former result is in contrast to the prediction of phenomenological theories of a sensitive dependence upon the amount of hexagonal formers (16). While the absolute energy is little affected by the addition of hexagonal formers, we found that their asymmetric distribution caused the stalk to become a metastable intermediate, which would allow fusion to become a two-step, rather than one-step, thermally activated process.

Certainly the most important result of our calculation is the following: although the fusion process remains one with two barriers, one due to stalk formation and another that depends upon the specific mechanism, the second barrier is rapidly reduced by the addition of hexagonal former of greater abundance in the *cis* layer to a value comparable to that of the initial stalk itself. As emphasized earlier, the calculated energy of the stalk is rather small, $\sim 5\ k_BT$ in our copolymer system, corresponding to 13 k_BT in a biological membrane.

We note that the volume fraction of hexagonal former in the *cis* leaf at which the two barriers become approximately equal occurs in our model at a value of $\sim\phi_2^{cis}\sim 0.43$. The average fraction of hexagonal formers in the bilayer is 0.35. Under the assumption of equal molecular weights for the *A* and *B* components of the diblock, these volume fractions correspond to a mole fraction of 0.47 in the *cis* leaf of a bilayer whose average mole fraction is 0.39. Again, the mole fractions of hexagonal formers in the membrane of human red blood cells are ~ 0.54 in the *cis* leaf and 0.35 when averaged over both leaves of the bilayer. Thus equality of the two barriers occurs in our model at a somewhat smaller asymmetry between leaves than occurs in red blood cell membranes. As the asymmetry increases, the second barrier to fusion continues to decrease and eventually becomes negative. When this occurs in a bilayer under zero surface tension, the bilayer is unstable. In the system shown in Fig. 9, this instability occurs at a mole fraction of hexagonal former in the *cis* layer of ~ 0.50.

We examined both the standard, hemifusion diaphragm pathway to fusion, and the more recently proposed stalk-hole pathway. In the system with the mixture of lamellar and hexagonal formers similar to that of red-blood cell membranes, we found that the barriers to fusion in the two mechanisms did not differ greatly, with those in the new mechanism being slightly lower. This would indicate that fusion could proceed by either pathway. In the standard mechanism, fusion is nonleaky. In the stalk-hole mechanism it can be leaky. The small values of α, the fraction of hole surrounded by the stalk when fusion occurs, which were obtained in the preceding section certainly would bolster the possibility of leakage. However, as Eastman et al. (21) already noted, even though fusion between model membranes is generally leaky, ''. . .systems exhibiting asymmetric transbilayer distributions of lipid clearly have the potential to be self-regulating and possibly to exhibit leak-tight fusion. . . . It will be of particular interest to determine the leakiness of fusion events in such systems.'' This work strongly reinforces that observation.

Our results predict that the rate of fusion in asymmetric systems depends nonlinearly on the volume fraction of hexagonal formers in the *cis* layer. This results from at least two effects. First, even linear changes of energy barriers with volume fraction of hexagonal former translate into nonlinear changes of fusion rates because fusion is a thermally activated process. This nonlinear behavior is in accord with the results of Eastman et al. (21). Second we found in our system resembling DOPC, DOPE mixtures with a fixed average composition that the stalk intermediate became metastable only when the asymmetry attained a certain minimum value. At that point, the fusion rate is expected to increase significantly.

To reiterate, our major result is that the two barriers to fusion are comparable and small for an amount of hexagonal former found in the *cis* layer, which does not differ greatly from that found in red blood cell membranes. One important implication of this result is that fusion should proceed readily once external sources have brought the membranes sufficiently close to initiate the process. Our results have been obtained by examining planar bilayers, and for the study of the fusion of endocytotic vesicles with the plasma membrane, the large curvature of the vesicles should probably be taken into account (36,37), something that can be done within the self-consistent field theory we have employed. However, it is known that such a curvature only enhances the fusion rate (38), and so the process should again proceed

readily once vesicle and membrane are brought to an optimum distance.

The observation that fusion should proceed quickly once the membranes are brought sufficiently close naturally leads to the question of how the energies of fusion intermediates depend upon the distance between the two tense membranes, which might fuse. This is an issue we shall address in a later publication.

We are grateful to Kirill Katsov for useful correspondence.

This work was supported by the National Science Foundation under grant No. 0503752.

REFERENCES

1. Chernomordik, L. V., and M. M. Kozlov. 2003. Protein-lipid interplay in fusion and fission of biological membranes. *Annu. Rev. Biochem.* 72:175–207.
2. Cohen, F. S., and G. B. Melikyan. 2004. The energetics of membrane fusion from binding, through hemifusion, pore formation, and pore enlargement. *J. Membr. Biol.* 199:1–14.
3. Evans, K. O., and B. R. Lentz. 2002. Kinetics of lipid rearrangements during poly(ethylene glycol)-mediated fusion of highly curved unilamellar vesicles. *Biochemistry.* 41:1241–1249.
4. Kozlov, M. M., and V. S. Markin. 1983. Possible mechanism of membrane fusion. *Biofizika.* 28:255–261.
5. Müller, M., K. Katsov, and M. Schick. 2002. New mechanism of membrane fusion. *J. Chem. Phys.* 116:2342–2345.
6. Müller, M., K. Katsov, and M. Schick. 2003. A new mechanism of model membrane fusion determined from Monte Carlo simulation. *Biophys. J.* 85:1611–1623.
7. Stevens, M. J., J. Hoh, and T. Woolf. 2003. Insights into the molecular mechanism of membrane fusion from simulation: evidence for the association of splayed tails. *Phys. Rev. Lett.* 91:188102–1–188102–4.
8. Marrink, S. J., and A. E. Mark. 2003. The mechanism of vesicle fusion as revealed by molecular dynamics simulations. *J. Am. Chem. Soc.* 125:11144–11145.
9. Smeijers, A. F., A. J. Marvoort, K. Pieterse, and P. A. J. Hilbers. 2006. A detailed look at vesicle fusion. *J. Phys. Chem. B.* 110:13212–13219.
10. Siegel, D. P. 1993. Energetics of intermediates in membrane fusion: comparison of stalk and inverted micellar intermediate mechanisms. *Biophys. J.* 65:2124–2140.
11. Kuzmin, P. I., J. Zimmerberg, Y. A. Chizmadzhev, and F. S. Cohen. 2001. A quantitative model for membrane fusion based on low-energy intermediates. *Proc. Natl. Acad. Sci. USA.* 98:7235–7240.
12. Noguchi, H., and M. Takasu. 2001. Fusion pathways of vesicles: a Brownian dynamics simulation. *J. Chem. Phys.* 115:9547–9551.
13. Katsov, K., M. Müller, and M. Schick. 2006. Field theoretic study of bilayer membrane fusion: II. Mechanism of a stalk-hole complex. *Biophys. J.* 90:915–926.
14. Lentz, B. 2006. Seeing is believing: the stalk intermediate. *Biophys. J.* 91:2747–2748.
15. Markin, V. S., and J. P. Albanesi. 2002. Membrane fusion: stalk model revisited. *Biophys. J.* 82:693–712.
16. Kozlovsky, Y., and M. M. Kozlov. 2002. Stalk model of membrane fusion: solution of energy crisis. *Biophys. J.* 82:882–895.
17. Katsov, K., M. Müller, and M. Schick. 2004. Field theoretic study of bilayer membrane fusion: I. Hemifusion mechanism. *Biophys. J.* 87: 3277–3290.
18. Rothman, J. E., and J. Lenard. 1977. Membrane asymmetry. *Science.* 195:743–753.
19. Devaux, P. 1991. Static and dynamic lipid asymmetry in cell membranes. *Biochemistry.* 30:1163–1173.
20. Seigneuret, M., and P. F. Devaux. 1984. Asymmetric distribution of spin-labeled phospholipids in the erythrocyte membrane: relation to shape changes. *Proc. Natl. Acad. Sci. USA.* 81:3751–3755.
21. Eastman, S., M. J. Hope, K. Wong, and P. R. Cullis. 1992. Influence of phospholipid asymmetry on fusion between large unilamellar vesicles. *Biochemistry.* 31:4262–4268.
22. Bailey, A. L., and P. R. Cullis. 1994. Modulation of membrane fusion by asymmetric transbilayer distributions of amino lipids. *Biochemistry.* 33:12573–12580.
23. Chernomordik, L., M. Kozlov, and J. Zimmerberg. 1995. Lipids in biological membrane fusion. *J. Membr. Biol.* 146:1–14.
24. Hope, M. J., and P. R. Cullis. 1980. Effects of divalent cations and pH on phosphatidylserine model membranes: a ^{31}P NMR study. *Biochem. Biophys. Res. Commun.* 92:846–852.
25. Gruner, S. M. 1989. Stability of lyotropic phases with curved interfaces. *J. Phys. Chem.* 93:1562–1570.
26. Siegel, D. P. 1986. Inverted micellar intermediates and the transitions between lamellar, inverted hexagonal, and cubic lipid phases. II. Implications for membrane-membrane interactions and membrane fusion. *Biophys. J.* 49:1171–1183.
27. Hope, M. J., D. C. Walker, and P. Cullis. 1983. Ca^{2+} and pH induced fusion of small unilamellar vesicles consisting of phosphatidylethanolamine and negatively charged phospholipids: a freeze fracture study. *Biochem. Biophys. Res. Commun.* 110:15–22.
28. Kozlovsky, Y., L. V. Chernomordik, and M. M. Kozlov. 2002. Lipid intermediates in membrane fusion: formation, structure, and decay of hemifusion diaphragm. *Biophys. J.* 83:2634–2651.
29. Li, X.-J., and M. Schick. 2000. Distribution of lipids in nonlamellar phases of their mixtures. *J. Chem. Phys.* 112:6063–6072.
30. Discher, B. D., Y.-Y. Won, D. S. Ege, J. C.-M. Lee, F. S. Bates, D. E. Discher, and D. A. Hammer. 1999. Polymersomes: tough vesicles made from diblock copolymers. *Science.* 284:1143–1146.
31. Loison, C., M. Mareschal, and F. Schmid. 2004. Pores in bilayer membranes of amphiphilic molecules: coarse-grained molecular dynamics simulations compared with simple mesoscopic models. *J. Chem. Phys.* 121:1890–1900.
32. Tolpekina, T., W. den Otter, and W. Briels. 2004. Simulations of stable pores in membranes: system size dependence and line tension. *J. Chem. Phys.* 121:8014–8020.
33. Tieleman, D., H. Leontiadou, A. Mark, and S. Marrink. 2003. Simulation of pore formation in lipid bilayers by mechanical stress and electric fields. *J. Am. Chem. Soc.* 125:6382–6383.
34. Leontiadou, H., A. Mark, and S. Marrink. 2004. Molecular dynamics simulations of hydrophilic pores in lipid bilayers. *Biophys. J.* 86:2156–2164.
35. Groot, R., and K. Rabone. 2001. Mesoscopic simulation of cell membrane damage, morphology change and rupture by nonionic surfactants. *Biophys. J.* 81:725–736.
36. Malinin, V. S., and B. R. Lentz. 2004. Energetics of vesicle fusion intermediates: comparison of calculations with observed effects of osmotic and curvature stresses. *Biophys. J.* 86:2951–2964.
37. Kasson, P., N. Kelley, N. Singhal, M. Vrlic, A. T. Brunger, and V. S. Pande. 2006. Ensemble molecular dynamics yields submillisecond kinetics and intermediates of membrane fusion. *Proc. Natl. Acad. Sci. USA.* 103:11916–11921.
38. Malinin, V. S., P. Frederik, and B. R. Lentz. 2002. Osmotic and curvature stress affect peg-induced fusion of lipid vesicles but not mixing of their lipids. *Biophys. J.* 82:2090–2100.